INL/JOU-19-55263-Revision-1

A Quantitative Failure Analysis on Capacity Fade in Rechargeable Lithium Metal Cells

Boryann Liaw, Eric J Dufek, Charles C Dickerson, Yulun Zhang, Qiang Wang, Shrikant Nagpure

February 2020

The INL is a U.S. Department of Energy National Laboratory
operated by Battelle Energy Alliance

INL/JOU-19-55263-Revision-1

A Quantitative Failure Analysis on Capacity Fade in Rechargeable Lithium Metal Cells

Boryann Liaw, Eric J Dufek, Charles C Dickerson, Yulun Zhang, Qiang Wang, Shrikant Nagpure

February 2020

Idaho National Laboratory
Idaho Falls, Idaho 83415

http://www.inl.gov

Prepared for the
U.S. Department of Energy
Office of Energy Efficiency and Renewable Energy, Office of Nuclear Energy
Under DOE Idaho Operations Office
Contract DE-AC07-05ID14517, DE-AC07-05ID14517

A Quantitative Failure Analysis on Capacity Fade in Rechargeable Lithium Metal Cells

Yulun Zhang, Qiang Wang, Boryann Liaw*, Shrikant C. Nagpure, Eric J. Dufek, Charles C. Dickerson

Energy Storage and Advanced Vehicles
Energy and Environmental Science and Technology
Idaho National Laboratory
Idaho Falls, ID 83415, USA
* E-mail: Boryann.liaw@inl.gov; (208) 526-3238.

Keywords: Rechargeable lithium metal batteries; Lithium metal electrode; Charge retention; Capacity fade; State of charge; Failure mode and effect analysis (FMEA)

Abstract

Rechargeable lithium battery (RLB) technology is transforming portable devices, vehicle electrification, and grid modernization. To make RLB durable, reliable and safe, conducting failure mode and effect analysis (FMEA) to identify failure mechanism under the operating conditions is very desirable. However, this ability is often overlooked or even lacking. The FA is often conducted by laboratory testing and postmortem analysis, and the knowledge typically empirical. Here we present a quantitative approach for FMEA that can reveal how failure modes and effects reduce the capacity of a RLB. This approach is based on the state of the battery for FMEA, contrary to the conventional approach based on operating or testing conditions. The key aspect of this FMEA method is to convert the experimental results to a state-of-charge (SOC)-based analytic methodology. Such a conversion can separate the thermodynamic and kinetic attributes of capacity fade based on compositional correspondence in the electrode, so the loss and the decreased utilization of the active materials can be determined respectively.

1 Introduction

Li metal electrode (LME) is considered the "holy grail" for high-energy rechargeable Li batteries (RLB) designs that can surpass 350 Wh kg^{-1} for electric vehicle applications [1-4]. Yet, to date almost all possible designs encounter cycle life issues associated with LME performance. The conventional approach to understand LME performance relies on electrochemical testing of the cells. This approach measured capacity fade under various experimental conditions and determine the cause of the fading by physicochemical characterizations of the electrode materials. The results are empirical, and the lack of quantitative correlation between the amount of capacity fade and the degree of severity caused by the fading mechanism is prohibiting effective improvements to aid battery performance today. A comprehensive, reliable analytic diagnosis on cell performance using an electrochemical evaluation technique is highly desired to enable battery researchers to understand the test results in order to improve their approach in solving technical issues.

Although the underlying failure mechanisms associated with LME are known for some time, and they are primarily due to the solid electrolyte interphase (SEI) formation that consumes the electrolyte. In addition, excessive SEI formation could lead to isolation of some Li metal into "inactive" or "dead Li." The interplay of SEI and "dead Li" formation caused the loss of Li inventory (LLI). More devastatingly, this process changed the surface morphology and roughness of the LME significantly, as well as increased porosity in the bulk of LME cycle by cycle. This vicious cycle also disturbed electrolyte distribution in the cell and further increased the electrolyte depletion [3,5-8]. There is little success to quantify these attributes to improve cycle life. To extend cycle life and sustain reliable operation of these RLBs, there is an urgent need to identify and quantify failure modes and effects on the performance of LME *in situ* and *operando* [9-15]. Here, we introduce an accurate and precise "electrochemical analytic diagnosis (eCAD)" method to determine the attributes and amount of capacity loss in LME-based RLB during cycle aging. This method clearly identifies and quantifies capacity fade due to (1) loss of active materials (LAM) and LLI (which are thermodynamic attributes) and (2) under-utilization of the electrode active materials (UAM) due to rate-dependent polarization (IR) and additional transport-related kinetic polarization hindrance (KPH)—all kinetic attributes. This method offers a comprehensive comparison and data analytic capability superior to the prior arts, such as those using incremental capacity analysis (dQ/dV) or alike [8,16-19]. This approach emphasizes thermodynamic state determination to derive accurate interpretation and inference of the experimental data based on the state-of-charge (SOC) changes in the cell and the performance under the influence of operating conditions. Such knowledge is very useful for developing proper guidance to improve RLB design and operation. The knowledge gained from the

thermodynamic aspect should be more universal for the cell chemistry than those from the kinetic aspects (that are sensitive to cell design metrics and dimensional scales that extend from materials, electrodes, to cell). Since this approach is quantitative, a failure mode can be identified and its effect on performance quantified. Furthermore, any deviations observed in the operating or testing conditions can be easily aligned with the performance metrics of the cell at a defined state. Such a thermodynamic state-based failure mode and effect analysis (FMEA) on RLB functions is non-invasive and *in operando*. The ability to quantify failure modes and effects as a function of the "state of the system" is unique and beneficial for practical applications.

2 Experimental

***Cell Build**:* Electrolyte was prepared by dissolving 1.2 M lithium hexafluorophosphate ($LiPF_6$, Kishida) into a 3:7 (w/w) mixture of ethylene carbonate (EC, BASF) and ethyl methyl carbonate (EMC, BASF) with 2 wt% vinylene carbonate (VC, BASF). The positive electrode laminates were acquired from the Cell Analysis, Modeling and Prototyping (CAMP) facility at Argonne National Laboratory (ANL). These laminates were prepared from blend of 90% $Li_xNi_{0.6}Mn_{0.2}Co_{0.2}O_2$ (NMC-622) with 5% Timcal C45 carbon black and 5% polyvinylidene fluoride (PVDF) binder. The laminates were cast on 20 μm thick Al foil with a loading of 10.03 mg cm^{-2} (including inactive components). The calendared thickness and porosity of the laminate was 58 μm (1.45 mAh cm^{-2} areal capacity) and 35% (based on loading), respectively. The LME used was 250 μm thick Li foil (MTI Corporation). Celgard 2500 was used as the separator, which is a porous polypropylene membrane with 55% porosity.

Prior to assembly all the CR2032 components, spacers, and spring were washed with ethanol in an ultrasonic bath for 15 minutes and dried at 60°C (at vacuum strength greater than –75 kPa) for a minimum of 8 h prior to introduction into the glovebox. A 1.43 cm diameter negative LME was punched from the Li foil and pasted on the spacer inside the glovebox. A 1.43 cm diameter of cathode disk was punched from the NMC-622 laminates and dried at 90°C (at vacuum strength greater than –75 kPa) for a minimum of 8 h prior to use. The disks were carefully weighed after transferring to the glovebox. Full cells of LME || NMC-622 in CR2032 coin-cell configuration were assembled inside an Argon filled glovebox with H_2O and O_2 level held below 0.2 ppm. The cells were filled with 14 μL electrolyte (5.8 g Ah^{-2}, ~3.16 times the total porosity in the separator and cathode) in a single aliquot and sealed with Hoshen crimper.

Cycle Aging Test Protocol and Schedule: The cells were cycled inside an environmental chamber set at 25°C using either a Maccor 4000 or a Bio-Logic cycler between 2.5 V (V_{min}) and 4.5 V (V_{max}). The testing protocol and schedule is shown in the flowchart in

Figure 1. The test schedule includes three formation cycles at C/10 rate. The capacity at the end of the third formation cycle was used as the nominal capacity of the cell. An initial Reference Performance Test (RPT-0) of the cell was conducted after the formation cycles. The RPT comprises one C/10 and one C/20 charge-discharge cycle to evaluate the utilization of the NMC cathode active material at these rates. Twenty five (25) charge-discharge cycles at C/3 for performance evaluation were commenced after RPT-0, followed by PRT-1. Such a schedule was continued every 25 cycles to determine the state-of-health of the cell and its capacity fade cycle by cycle.

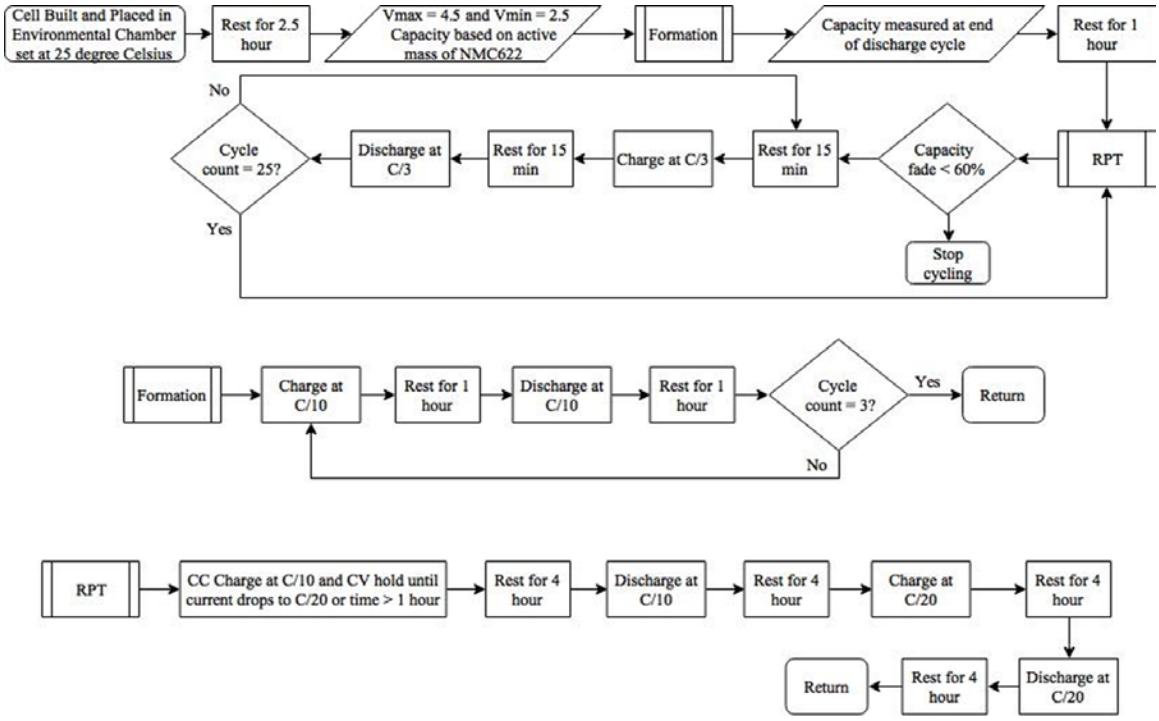

Figure 1. Cycle aging test protocols and schedule.

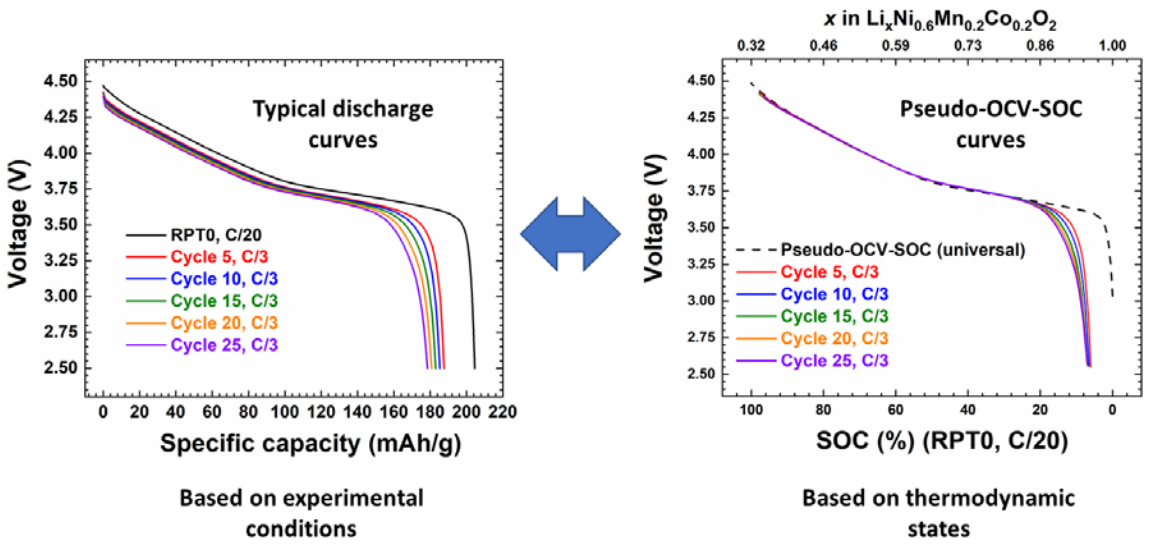

Figure 2. The unique aspect of the electrochemical analytic diagnosis (eCAD) technique: the ability to transform (a) a series of discharge curves of an LME || NMC-622 cell as a function of experimental conditions into (b) a series of thermodynamic state-of-charge (SOC) based analytic curves to reveal the attributes of the capacity fade during cycle aging.

3 The Electrochemical Analytic Diagnosis (eCAD) Technique

The unique aspect of the electrochemical analytic diagnosis (eCAD) technique is shown in Figure 2. Typical discharge curves from cycle aging experiments of a LME || NMC-622 coin cell at C/3 rate and 25°C are shown in Figure 2(a). Using this experiment as an example, we showed that these curves can be transformed into a series of SOC-based analytic discharge curves to display the changes of Li content in the NMC composition during cycle aging. The data transformation is illustrated in Figure 3.

3.1 Deriving SOC-Based Discharge Curves for Electrochemical Analytic Diagnosis

The eCAD method is a thermodynamic state-based FMEA technique. Key to implement this eCAD method successfully is the use of thermodynamic states as the basis to properly infer the nature of the capacity fade in cycle aging. Such a basis is established by a well-defined correspondence between cell open circuit voltage (OCV) and SOC, which is universal without bias of size, shape, weight of the cell and other cell design metrics including geometric dimensions, active material loading of the electrodes, porosity and active surface area in each electrode, properties of the separator and binder, etc. [16-20]. This OCV–SOC correspondence is a direct representation of the Gibbs free energy of the cell reaction (denoted as $\Delta G_{\text{NMC-622}}$) and the Li content in the active

material's composition in the NMC-622 electrode; or, in a simplified notation as: ΔG_x–x, where x is the Li content in NMC-622 in the pseudo-binary Li–NMC-622 system

This universal relationship lays the foundation for inferring Li content in NMC-622, as explained in a recent work by Li *et al*. [20]. Applying this principle in the eCAD method to the LME || NMC-622 cell, the following steps are used in the transformation of the analytic discharge curve:

Step 1) Derive the *pseudo*-OCV versus SOC curve from a set of charge discharge curves at C/20 (as in RPT-0). The principle and method to derive the *pseudo*-OCV–SOC curve has been described in prior work by Liaw and his co-workers [16-20], therefore we do not explain further herein. It is worth noting that this OCV–SOC curve can also be obtained by Galvanostatic Intermittent Titration Technique (GITT). However, prior study indicated that the two methods should yield a very similar curve. Whereas the GITT curve would be populated with and traced by only data points determined by the experiments, this *pseudo*-OCV versus SOC curve obtained from the averaging of the charging and discharging curves gives the full characteristic over the entire SOC range. Thus, it is much more convenient and useful to use this averaging method of C/20 charging and discharging curves to yield the *pseudo*-OCV–SOC curve.

Step 2) Transform a typical discharge curve at C/3 into an IR-free voltage ($V_{IR\text{-}free}$) versus specific capacity profile (a $V_{IR\text{-}free}$–$Q_{C/3}$ curve) and then further into a $V_{IR\text{-}free}$ versus depth of discharge (DOD) profile (a $V_{IR\text{-}free}$–DOD curve @C/3). Here, the effect of polarization is removed as much as possible to attain an approximated state that is close to the *pseudo*-OCV.

Step 3) Transform the $V_{IR\text{-}free}$–DOD curve @C/3 into that @C/20 to correlate the $V_{IR\text{-}free}$–DOD curve @C/20 to the universal *pseudo*-OCV–SOC curve. Here, the capacity measured in the experiment is mapped to DOD first and then aligned with SOC. Using Cycle 25 discharge curve at C/3 in Figure 3(c) as an example, at the end of discharge (EOD) the DOD is 100% at C/3. However, this $Q_{C/3}$ at 100% DOD is only 87.3% DOD in $Q_{C/20}$.

This transformation of DOD from $Q_{C/3}$ to $Q_{C/20}$ allows us to align the curve with the *pseudo*-OCV–SOC at any point in time through cycle aging to reveal the failure modes and effects in the cell. This approach could also be applied to calendar aging studies with RPTs. This process allows us decipher if a deviation in the cell performance is related to (1) the Li content in the cathode (NMC-622) composition to determine the amount of materials loss (LAM and/or LLI)—thermodynamic origins—or (2) UAM due to rate-dependent IR or KPH as an attribute arisen from additional polarization effects at the corresponding SOC as revealed by the $V_{IR\text{-}free}$ in the experiments—kinetic origins.

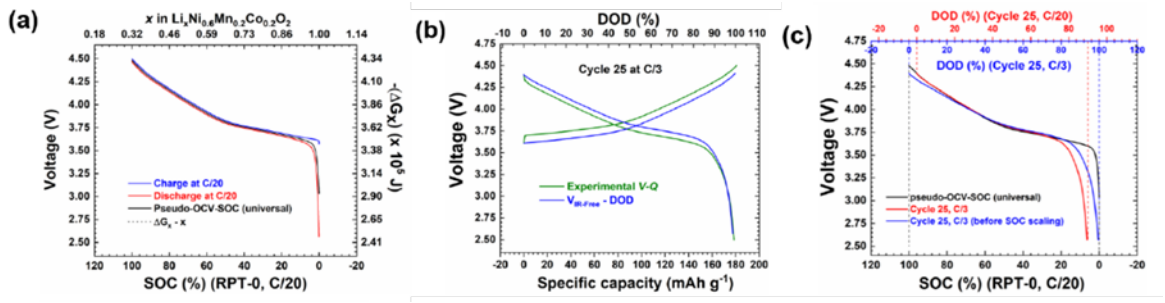

Figure 3. Schematic showing the steps involved in the FMEA analytics using the state of cell to analyze capacity fade in an LME || NMC-622 cell.

4 Understanding the FMEA on an LME || NMC-622 Cell

Figure 4 shows the capability of this thermodynamic state or SOC-based FMEA on a sample cell that behaved as anticipated from the cell design in the build. In Figure 4(a) the SOC-based analytic discharge curves from RPT-0 to RPT-1 along with the *pseudo*-OCV–SOC curve are shown and the variations displayed as highlighted by gold colored circular lines. Figure 4(b) further shows that, as the discharge rate increased from C/20 to C/3, additional UAM attributes to the capacity loss could be revealed.

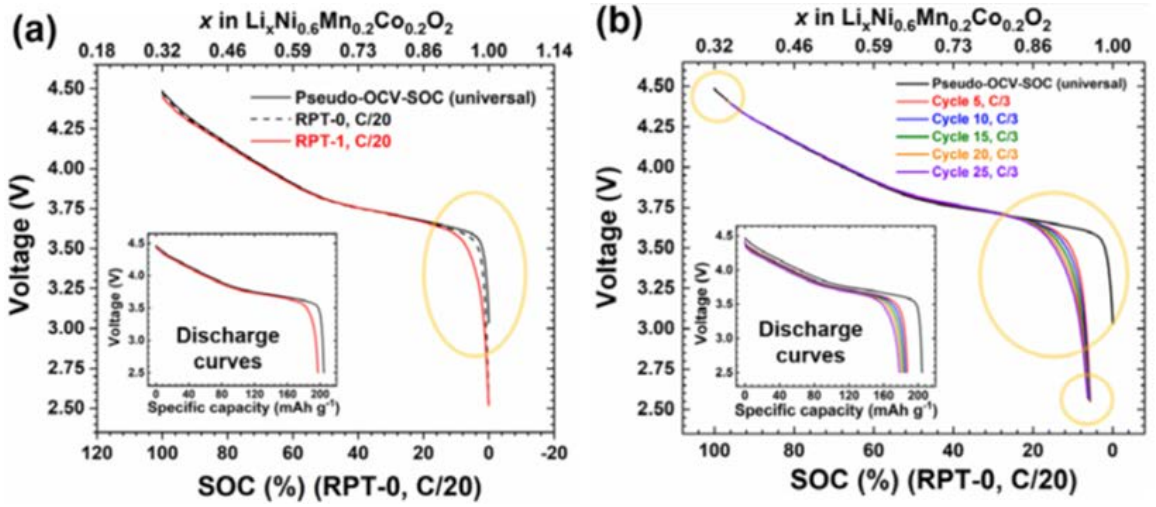

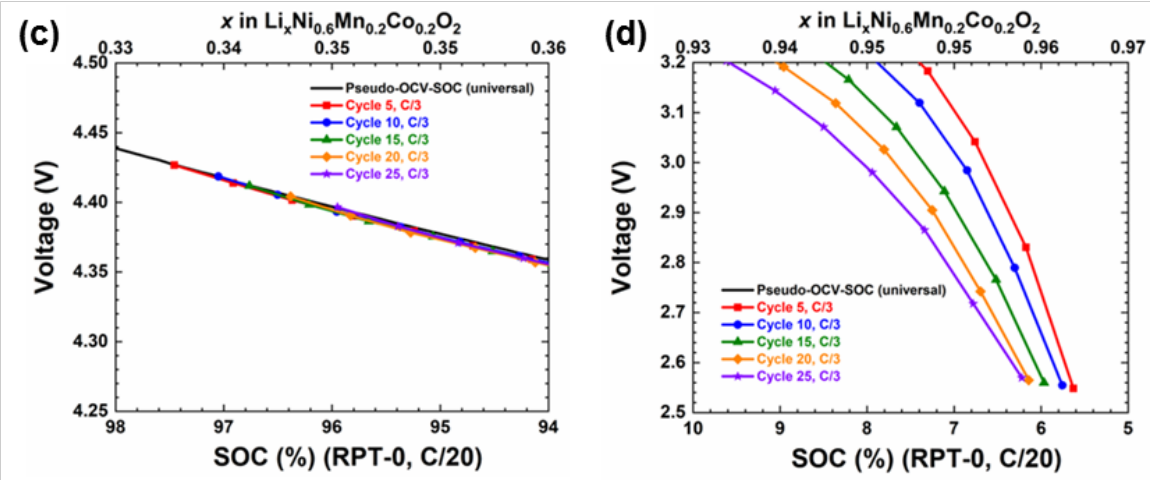

Figure 4. FMEA on an LME || NMC-622 cell for revealing rate dependent capacity fade (*QF*) during cycle aging. (a) State changes in two reference performance tests (RPT-0 to RPT-1, C/20). (b) Evolution of the state in five discharge regimes at C/3: Cycle 5, 10, 15, 20 and 25 over the cycle aging. The insets are the corresponding discharge curves for comparison. The areas, as highlighted by the circular translucent orange color in (b), are displayed in greater details in (c) beginning of discharge (BOD) and (d) end of discharge (EOD) where distinct features that reveal fading phenomena attributed to *QF* can be easily observed.

Table 1 provides more detailed information of the FMEA on the capacity fade (*QF*) and its attributes. The results are summarized as follows:

a) $QF_{LAM@C/20}$—The $Q_{C/20}$ fade from RPT-0 to RPT-1—is attributed to the loss of active material (LAM) in NMC-622 based on the following considerations:
   i. The Li supply from LME is in significant excess in the cell build. There is no evidence to suggest that the Li supply was constrained in the first period of 25-cycle aging.
   ii. As shown in Figure 4(a), the terminal compositions of NMC at the beginning of discharge (BOD) and EOD were almost identical in both RPTs. This result indicates the capacity came from the same compositional range in each test. Thus, if there were the same amount of NMC active material, we would expect to receive the same capacity. The difference in $Q_{C/20}$ from RPT-0 to RPT-1 therefore must be an active material loss.
   iii. However, one can arguably saying that the SOC-based analytic discharge curves also indicated that KPH might have affected the utilization of NMC-622 (UAM) below 20% SOC. Therefore, we cannot rule out the possibility of KPH that could also attribute to the capacity fade at C/20 ($QF_{KPH@C/20}$). What

caused KPH cannot be concluded as yet, but a couple of usual suspects related to mass transport could be speculated. If so, QF_{KPH} could be recurring but unlikely accumulative.

iv. Furthermore, based on the discussion below and Table 1, there are additional $QF_{IR@C/3}$ and $QF_{KPH@C/3}$ besides $QF_{LAM@C/20}$. If $QF_{LAM@C/20}$ were $QF_{KPH@C/20}$, then $QF_{KPH@C/3}$ and $QF_{KPH@C/20}$ would have very similar quantities, at least on the same order of magnitude. It is unlikely that QF_{KPH} is rate independent, especially between C/3 and C/20. Therefore, based on (iii) and (iv) we tend to rule out the possibility that $QF_{KPH@C/20}$ should account for $QF_{LAM@C/20}$.

On average $QF_{LAM@C/20}$ occurred on the order of 0.26 mAh g^{-1} per cycle or 6.61 mAh g^{-1} over the entire 25 cycles of C/3 aging (if the loss were not linear).

b) $QF_{IR@C/3}$—an ohmic dc resistance (IR drop)-induced capacity fade, an artifact due to rate-dependent UAM—is estimated on the order of 14.36 mAh g^{-1} recurring in each cycle at C/3 for this cell. This quantity is estimated from the difference between the first cycle $Q_{C/3}$ and the $Q_{C/20}$ that was determined in RPT-0. Here we assume:

   i. The ohmic dc resistance of the cell is rather constant over the SOC range studied in the cycle aging. This series resistance should include all conductive parts associated with the electrical current in the solids along the cell reaction pathway and the ionic current in the bulk electrolyte and in most cases in the electrode's porous media. We should note that the data acquisition rate and the slew rate of the tester's power electronics could affect the precision of the measurements, and we have paid attention to such issues in our analyses.

   ii. At this stage of life, the morphology and electrode architecture of the NMC-622 cathode should not alter significantly to affect the electrode kinetics or mass transport in the pore structure of the cathode.

   iii. Likewise, the morphology of LME and Li deposition and stripping rates also stay relatively stable in the first period of 25-cycle aging for the cell.

c) $QF_{KPH@C/3}$—an additional under-utilization of the NMC-622 cathode due to C/3 cycle aging—additional capacity fade on an order of magnitude similar to $QF_{LAM@C/20}$ but cannot be accounted for by the previous two origins. This quantity increases with cycle number in a linear fashion in the first period of 25-cycle aging, as shown in Table 1. It is also worth noting that $QF_{KPH@C/3}$ does change the terminal SOC at EOD cycle by cycle, unlike $QF_{LAM@C/20}$ which does not.

QF attributes (a)−(c) are consistent with the results exhibited in Figure 4(b), where the cathode utilization near the end of discharge (below 30% SOC) began to show the toll of KPH as the rate increased from C/20 to C/3 and cycle by cycle, where QF_{LAM} and QF_{KPH}, increase with cycle number. The sum of these losses as shown in the charge retention curve is rather linear.

Table 1. Detailed capacity fade attributes quantified by the FMEA from RPT-0 to RPT-1.

Cycle	Capacity (Q)	Loss of active material (QF_{LAM})	IR-induced UAM (QF_{IR})	KPH-induced UAM (QF_{KPH})
RPT-0 (C/20)	204.52	0.00	—	—
Cycle 1	189.90	0.26	14.36	0.00
Cycle 5	187.61	1.32	14.36	1.24
Cycle 10	185.31	2.64	14.36	2.21
Cycle 15	183.02	3.97	14.36	3.18
Cycle 20	180.81	5.29	14.36	4.07
Cycle 25	178.51	6.61	14.36	5.04
RPT-1 (C/20)	197.38	7.14	—	—
Cycle 26	177.15	7.32	14.36	5.70
Cycle 30	175.28	8.02	14.36	6.86
Cycle 35	172.99	8.90	14.36	8.28
Cycle 40	170.44	9.78	14.36	9.95
Cycle 45	168.23	10.67	14.36	11.27
Cycle 50	166.27	11.55	14.36	12.35
RPT-2 (C/20)	192.62	11.90	—	—

Note: all quantities in Q or QF are in mAh g^{-1}.

Two unique aspects of this FMEA approach should be noted here:

a) The point-to-point detection of deviations in $V_{IR\text{-}free}$ as a function of SOC in the course of cell reaction is a consistent and reliable assessment of Li content in the NMC-622 cathode. This capability offers the basis for a clear identification of all capacity fade attributes and may offer the possibility to determine the Li inventory in LME, NMC cathode, and SEI formation with the electrolyte.
b) This FMEA method applies thermodynamic principles to providing a reliable framework for accurate and precise fault detection in a quantitative manner.

5 Conclusion

We have shown the charge retention performance of a rechargeable Li metal cell and its cycle aging behavior. We used this sample cell to illustrate a quantitative failure mode and effect analysis (FMEA) based on thermodynamic state determination. Precise and accurate FMEA was demonstrated by true state-of-charge (SOC) correspondence and quantitative analysis of capacity fade (QF) attributes. These QF attributes include those from (1) the loss of active materials in the cathode (QF_{LAM}), (2) IR-induced, rate-

dependent under-utilization of capacity (QF_{IR}), and (3) constrained transport-induced kinetic polarization hindrance that leads to increased under-utilization of the active material (QF_{KPH}) in the cathode. A reliable FMEA has been achieved to show the potential of this electrochemical analytic diagnosis method for guarding reliable and safe battery operation with the ability to monitor capacity fading attributes quantitatively.

6 Acknowledgements

This work has been partially supported by the Assistant Secretary for Energy Efficiency and Renewable Energy, Office of Vehicle Technologies of the U.S. Department of Energy through the Advanced Battery Materials Research (BMR) Program (Battery500 Consortium). Idaho National Laboratory is operated by Battelle Energy Alliance under Contract Nos. DE- DE-AC07-05ID14517 for the U.S. Department of Energy. The United States Government retains and the publisher, by accepting the article for publication, acknowledges that the United States Government retains a nonexclusive, paid-up, irrevocable, world-wide license to publish or reproduce the published form of this manuscript, or allow others to do so, for United States Government purposes. The data analytics part of the work has been partially supported by the Laboratory Directed Research and Development (LDRD) program at INL (Project No.: 19P45-013FP). The authors would like to thank the Cell Analysis, Modeling and Prototyping (CAMP) facility at Argonne National Laboratory (ANL) for providing the cathode laminates used in this work.

7 References:

1. J. Liu, Z. N. Bao, Y. Cui, E. J. Dufek, J. B. Goodenough, P. Khalifah, Q. Y. Li, B. Y. Liaw, P. Liu, A. Manthiram, Y. S. Meng, V. R. Subramanian, M. F. Toney, V. V. Viswanathan, M. S. Whittingham, J. Xiao, W. Xu, J. H. Yang, X. Q. Yang and J. G. Zhang, *Nat. Energy*, **4**, 180 (2019).
2. M. M. Thackeray, C. Wolverton and E. D. Isaacs, *Energy Environ. Sci.*, **5**, 7854 (2012).
3. C. J. Niu, H. L. Pan, W. Xu, J. Xiao, J. G. Zhang, L. L. Luo, C. M. Wang, D. H. Mei, J. S. Meng, X. P. Wang, Z. Liu, L. Q. Mai and J. Liu, *Nat. Nanotechnol.*, **14**, 594 (2019).
4. C. J. Niu, H. Lee, S. R. Chen, Q. Y. Li, J. Du, W. Xu, J. G. Zhang, M. S. Whittingham, J. Xiao and J. Liu, *Nat. Energy*, **4**, 551 (2019).
5. D. Aurbach, E. Zinigrad, Y. Cohen and H. Teller, *Solid State Ionics*, **148**, 405 (2002).

6. M. Nagasaki, K. Nishikawa and K. Kanamura, *J. Electrochem. Soc.*, **166**, A2618 (2019).
7. Y. Wang, L. Fu, L. Shi, Z. Wang, J. Zhu, Y. Zhao and S. Yuan, *ACS Appl. Mater. Interfaces*, **11**, 5168 (2019).
8. K.-H. Chen, K. N. Wood, E. Kazyak, W. S. LePage, A. L. Davis, A. J. Sanchez and N. P. Dasgupta, *J. Mater. Chem. A*, **5**, 11671 (2017).
9. K. Yan, J. Y. Wang, S. Q. Zhao, D. Zhou, B. Sun, Y. Cui and G. X. Wang, *Angew. Chem. Int. Ed.* (2019).
10. M. Liu, Z. Cheng, K. Qian, T. Verhallen, C. Wang and M. Wagemaker, *Chem. Mater.*, **31**, 4564 (2019).
11. F. Hao, A. Verma and P. P. Mukherjee, *Energy Storage Mater.*, **20**, 1 (2019).
12. A. Aryanfar, D. J. Brooks, A. J. Colussi and M. R. Hoffmann, *Phys. Chem. Chem. Phys.*, **16**, 24965 (2014).
13. J. Steiger, D. Kramer and R. Moenig, *Electrochim. Acta*, **136**, 529 (2014).
14. B. Y. Liaw, Y. Wei and F. Wang, *Chapter 8: Managing Safety Risk by Cell Manufacturers from the book Electrochemical Power Sources: Fundamentals, Systems, and Applications: Li-Battery Safety*, United States (2018).
15. D. Doughty and E. P. Roth, *The Electrochem. Soc. Interface, Summer ed.*, 37 (2012).
16. M. Dubarry, V. Svoboda, R. Hwu and B. Y. Liaw, *ECS Solid State Lett.*, **9**, A454 (2006).
17. M. Dubarry, V. Svoboda, R. Hwu and B. Y. Liaw, *J. Power Sources*, **174**, 1121 (2007).
18. M. Dubarry and B. Y. Liaw, *J. Power Sources*, **194**, 541 (2009).
19. C. Truchot, M. Dubarry and B. Y. Liaw, *Appl. Energ.*, **119**, 218 (2014).
20. Z. Li, J. Huang, B. Y. Liaw and J. Zhang, *J. Power Sources*, **348**, 281 (2017).

Figure Captions

Figure 1. Cycle aging test protocols and schedule.

Figure 2. The unique aspect of the electrochemical analytic diagnosis (eCAD) technique: the ability to transform (a) a series of discharge curves of an LME || NMC-622 cell as a function of experimental conditions into (b) a series of thermodynamic state-of-charge (SOC) based analytic curves to reveal the attributes of the capacity fade during cycle aging.

Figure 3. Schematic showing the steps involved in the FMEA analytics using the state of cell to analyze capacity fade in an LME || NMC-622 cell.

Figure 4. FMEA on an LME || NMC-622 cell for revealing rate dependent capacity fade (*QF*) during cycle aging. (a) State changes in two reference performance tests (RPT-0 to RPT-1, C/20). (b) Evolution of the state in five discharge regimes at C/3: Cycle 5, 10, 15, 20 and 25 over the cycle aging. The insets are the corresponding discharge curves for comparison. The areas, as highlighted by the circular translucent orange color in (b), are displayed in greater details in (c) beginning of discharge (BOD) and (d) end of discharge (EOD) where distinct features that reveal fading phenomena attributed to *QF* can be easily observed.

Table Captions

Table 1. Detailed capacity fade attributes quantified by the FMEA from RPT-0 to RPT-1.